

Accelerator-mode islands and superdiffusion in double-kicked rotor

Fengdi Wang(王风涤) and Ping Fang(方萍)

Citation: Chin. Phys. B, 2023, 32 (**6**): 060504. DOI: 10.1088/1674-1056/accb4b
Journal homepage: http://cpb.iphy.ac.cn; http://iopscience.iop.org/cpb

What follows is a list of articles you may be interested in

Unstable periodic orbits analysis in the Qi system

Lian Jia(贾莲), Chengwei Dong(董成伟), Hantao Li(李瀚涛), and Xiaohong Sui(眭晓红)
Chin. Phys. B, 2023, 32 (**4**): 040502. DOI: 10.1088/1674-1056/aca9c3

Asymmetric image encryption algorithm based ona new three-dimensional improved logistic chaotic map

Guo-Dong Ye(叶国栋), Hui-Shan Wu(吴惠山), Xiao-Ling Huang(黄小玲), and Syh-Yuan Tan
Chin. Phys. B, 2023, 32 (**3**): 030504. DOI: 10.1088/1674-1056/ac7dbb

A novel algorithm to analyze the dynamics of digital chaotic maps in finite-precision domain

Chunlei Fan(范春雷) and Qun Ding(丁群)
Chin. Phys. B, 2023, 32 (**1**): 010501. DOI: 10.1088/1674-1056/ac785c

Synchronously scrambled diffuse image encryption method based on a new cosine chaotic map

Xiaopeng Yan(闫晓鹏), Xingyuan Wang(王兴元), and Yongjin Xian(咸永锦)
Chin. Phys. B, 2022, 31 (**8**): 080504. DOI: 10.1088/1674-1056/ac5a43

The dynamics of a memristor-based Rulkov neuron with fractional-order difference

Yan-Mei Lu(卢艳梅), Chun-Hua Wang(王春华), Quan-Li Deng(邓全利), and Cong Xu(徐聪)
Chin. Phys. B, 2022, 31 (**6**): 060502. DOI: 10.1088/1674-1056/ac539a

---

SPECIAL TOPIC — Celebrating the 100th Anniversary of Physics Discipline of Xiamen University

Accelerator-mode islands and superdiffusion in double-kicked rotor

Fengdi Wang(王风涤)[1] and Ping Fang(方萍)[1,2,†]

[1] *School of Science, Beijing University of Posts and Telecommunications, Beijing* 100876, *China*
[2] *State Key Laboratory of Information Photonics and Optical Communications, Beijing* 100876, *China*

(Received 21 February 2023; revised manuscript received 23 March 2023; accepted manuscript online 7 April 2023)

This paper presents a theoretical investigation of the presence of acceleration islands in the phase space of double-kicked rotor (DKR) systems, which can lead to superdiffusive behavior. We establish the conditions for the existence of period-1 acceleration centers and subsequently calculate the stability conditions for both period-1 and period-2 accelerate mode islands. A detailed analysis of local and global diffusion in the vicinity of the islands and the stickiness regions is provided. It is demonstrated that the mean stickiness time decays exponentially when the phase point is located in the interior of the island. Moreover, the phase point undergoes a power-law decay with a power equal to approximately 5 when entering the sticky region. These findings offer a foundation for future exploration of quantum dynamics in the DKR system.

Keywords: superdiffuision, accelerator-mode islands, double-kicked rotor

PACS: 05.45.Ac, 05.60.Cd, 05.45.Mt, 45.05.+x **DOI:** 10.1088/1674-1056/accb4b

1. Introduction

Diffusion behaviors in Hamiltonian systems have emerged as a central topic in the study of chaotic dynamics.[1–10] It has been shown that diffusion behaviors are rooted in the structural properties in phase space. Specifically, localization corresponds to the Kolmogorov–Arnold–Moser (KAM) invariant tori and islands in phase space, while normal diffusion is related to the chaotic sea. A paradigmatic example is the kicked rotor model, also known as standard map or Chirikov map, which has rich diffusion dynamics depending on a nonintegrability parameter k.[11,12] For the small values of k, the motion in angular momentum direction is bounded by KAM-invariant tori, leading to localization: $t \to \infty$, $\langle \Delta p_t^2 \rangle \to t^\mu, \mu = 0$. When k is sufficiently large, the motion resembles a Brownian random walk, in which the chaotic region occupies the entire phase plane, resulting in normal diffusion in angular momentum space: $\langle \Delta p_t^2 \rangle = k^2/2t$.

However there are some intervals of k at $k \geq 2\pi$, in which the diffusion is not normal but superdiffusion instead ($\mu > 1$). This behavior is caused by the presence of accelerator modes:[13] there exist stable islands in phase space surrounding periodic orbits of period-1, and these orbits correspond to jumps in p equal to 2π or integer multiples of 2π. Orbits trapped inside these accelerator modes exhibit ballistic diffusion with $\mu = 2$. Moreover, orbits that are close to these islands and become temporarily trapped due to the stickiness of the surrounding neighborhood (containing cantori) also exhibit superdiffusion ($\mu > 1$). In addition to accelerator modes with a period of 1, higher period modes also exist, despite their influence decreases rapidly with increasing k.[11]

It has been observed that islands with accelerator modes can exhibit a self-similar structure.[14] These structures, formed by satellite elliptic orbits ordered in a chain around a periodic orbit, can be explained through renormalization and the Poincaré–Birkhoff theorem.[15–17] The presence of accelerator mode (AM) islands, even if they are a small fraction of the total phase space, can significantly affect global diffusion, leading to a global value of the diffusion exponent close to 2 and to the formation of alpha-stable Levy distributions.[11,12] Previous research has also studied the three characteristic times of the standard map: the Lyapunov characteristic time,[18] the mean Poincaré recurrence time,[19] and the stickiness time.[20–22] In addition, rotating accelerator-mode islands,[23] a new type of accelerator mode island at small k, has also been observed.

An important variant of the kicked rotor model, the double-kicked rotor (DKR) system,[24] has been the subject of much attention due to its interesting quantum dynamics and topological properties.[25–27] It has been found to exhibit superballistic and exponential diffusion in the pseudo-classical limit system.[28–30] However, the superdiffusion observed in these studies does not originate from accelerator islands, leaving it an open question whether AM islands and superballistic diffusion exist in the DKR system. We also provide a detailed simulation of the diffusion behavior in the stickiness region. Consider the correspondence between quantum and classical Hamiltonian systems,[28,31,32] our results may inspire further

†Corresponding author. E-mail: pingfang@bupt.edu.cn

© 2023 Chinese Physical Society and IOP Publishing Ltd

study of quantum dynamics in the DKR system.

The structure of the article is as follows: in Section 2 we briefly describe the DKR model and the relevant diffusion rate measurements. In Section 3 we use both theoretical and numerical methods to derive the location of AM islands and the conditions for the stable period-1 and period-2 AM islands. In Section 4 we present our main results of stickiness times. Finally, in Section 5 we summarize and conclude the main findings of this work.

2. Model

The kicked rotor is one of the most studied models of the chaos theory of Hamiltonian systems, which describes a particle rotating on a ring subjected to an instantaneous excitation by a periodic external field.[15] The Hamiltonian of this system is

$$H = \frac{p^2}{2} + k\cos(\theta)\sum_{n\in N}\delta(t-n\tau), \tag{1}$$

where θ and p are the angle and the angular momentum of the particle, the kick turned on instantaneously at multiples of τ with kicking strength k, which characterizes the nonintegrability of the system. Many properties of this mapping are universal for Hamiltonian systems, so Chirikov called it the standard map. The global superdiffusion in this model is caused by the stable accelerator mode islands (period-1) for some intervals of k:[2]

$$(2\pi a) \leqslant k \leqslant \sqrt{(2\pi a)^2+16}, \tag{2}$$

where a is a positive integer. The width of each interval reads[2]

$$\Delta k \approx 8/k. \tag{3}$$

The double-kicked rotor system is an important variant of the kicked rotor, *i.e.*, the rotor is subjected to another instantaneous kick in time τ. The time interval between the two kicks is η. This model was first proposed by Wei Li *et al.*,[24] for exploring the chaos control problem of classical Hamiltonian systems. The Hamiltonian and mapping of the system are as follows:

$$\begin{aligned} H = {} & \frac{p^2}{2} + k\cos(\theta)\sum_{n\in N}\delta(t-n\tau) \\ & + k\cos(\theta)\sum_{n\in N}\delta[t-(n\tau+\eta)]. \end{aligned} \tag{4}$$

Here we assume the two kicking strengths are the same. This map is still a conservative system. Here we consider the pseudo-classical limit DKR, whose quantum dynamics corresponds to a virtual classical dynamics under the quantum resonance condition ($\hbar\tau = 4\pi$, where $\hbar$ is the Planck constant) and pseudo-classical limit ($\hbar = 2\pi + \tilde{\hbar}$, $\tilde{\hbar}\to 0$, which $\tilde{\hbar}$ acting as a virtual Planck constant).[28] The quantum evolution can be expressed as a stroboscopic dynamics such that the wavefunction at time $t = n\tau$, $|\psi(t)\rangle$, is given by $|\psi(t)\rangle = \hat{U}_t|\psi(0)\rangle$, with the floquet operator

$$U = \exp\left(\mathrm{i}\frac{p^2}{2\hbar}\right)\exp\left(-\mathrm{i}\frac{k}{\hbar}\cos(\theta)\right)\exp\left(-\mathrm{i}\frac{p^2}{2\hbar}\right)\exp\left(-\mathrm{i}\frac{k}{\hbar}\cos(\theta)\right), \tag{5}$$

without loss of generality, we take $\eta = 1$. With the following rescaling:

$$P = p\tilde{\hbar}/\hbar, \quad K = k\tilde{\hbar}/\hbar, \tag{6}$$

and applying $\hbar = 2\pi + \tilde{\hbar}$, the floquet operator U can be deformed as

$$U = \exp\left[\frac{\mathrm{i}}{\tilde{\hbar}}\left(\frac{P^2}{2}+\pi P\right)\right]\exp\left[-\mathrm{i}\frac{K}{\tilde{\hbar}}\cos(\theta)\right]\exp\left[-\frac{\mathrm{i}}{\tilde{\hbar}}\left(\frac{P^2}{2}+\pi P\right)\right]\exp\left[-\mathrm{i}\frac{K}{\tilde{\hbar}}\cos(\theta)\right]. \tag{7}$$

It describes a rotor by the conjugate pair (θ, P). And implies that in the pseudo-classical limit of $\tilde{\hbar}\to 0$, this rotor undergoes a free rotation with the angular velocity $\mathrm{d}\theta/\mathrm{d}t = P+\pi$ or $-(P+\pi)$ alternatively between two consequential kicks, and the corresponding classical motion within a single step is given by the map

$$\begin{aligned} & P_n' - P_n = K\sin\theta_n, \\ & \theta_n' - \theta_n = P_n' + \pi, \\ & P_{n+1} - P_n' = K\sin\theta_n', \\ & \theta_{n+1} - \theta_n' = -P_{n+1} + \pi, \end{aligned} \tag{8}$$

where P_n' and θ_n' are two intermediate variables. The amount of change in momentum P after time $t = n\tau$ is

$$\Delta P(t/\tau) = P_{t/\tau} - P_0 = \sum_{n=0}^{t/\tau-1}(K\sin\theta_n + K\sin\theta_n'). \tag{9}$$

As chaotic dynamics emerges for $K \gg 1$, the position variables θ_n and θ_n' can be assumed to be ergodic on the interval $0 \leq \theta_n$, $\theta_n' \leq 2\pi$, and satisfy

$$\langle\sin\theta_n\rangle = 0, \quad \langle\sin\theta_n\sin\theta_{n'}\rangle = \frac{1}{2}\delta_{nn'},$$
$$\langle\sin\theta_n'\rangle = 0, \quad \langle\sin\theta_n'\sin\theta_{n'}'\rangle = \frac{1}{2}\delta_{nn'},$$

$$\langle \sin\theta_n \sin\theta'_{n'} \rangle = 0. \tag{10}$$

Therefore, for the number $n = t/\tau \gg 1$, the diffusion in angular momentum space can be calculated as

$$\langle \Delta P^2(n) \rangle \equiv 2D_{\rm eff} n = K^2 n, \tag{11}$$

where $\langle \cdot \rangle$ denotes the phase space average. Thus the diffusion coefficient $D_{\rm eff} = \frac{1}{2}K^2$.

The simulated relation between $D_{\rm eff}$ and K is plotted in Figs. 1(a) and 1(b) for large n. The data points of $D_{\rm eff}(K)$ that diverge from the normal diffusion (Eq. (11)), *i.e.* peaks, signify superdiffusion, which occurs on K near the integer multiple of π. We have also confirmed that superdiffusion ($1 < \mu < 2$) indeed appears at several K in Fig. 1(c). When normal diffusion occurs, the diffusion rate of DKR is greater than that of KR. The reason for this contrary result compared to other studies,[33] $\eta/\tau = (2\pi + \tilde{\hbar})/4\pi$ is very close to 1/2, rather than $\eta/\tau \ll 1$.

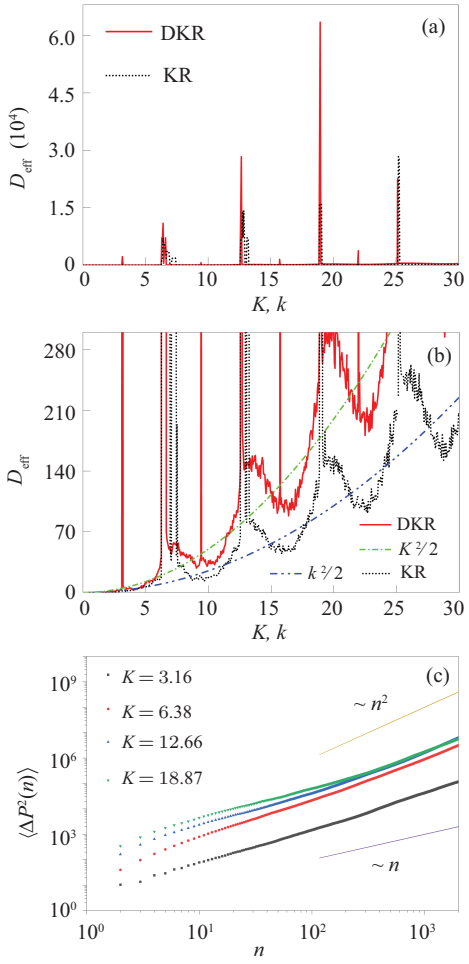


Fig. 1. (a) The simulated $D_{\rm eff}$ as a function of K (k), the initial conditions in the three diagrams above are taken uniformly over the entire phase space, with iteration steps $n = 2^4$. (b) The same result for $D_{\rm eff}$ in $[0, 280]$, compared with theoretical results for KR ($k^2/4$) and DKR ($K^2/2$). (c) The diffusion of angular momentum for several K corresponding to the peaks of $D_{\rm eff}$ in (a). The number of initial conditions is 4×10^4.

3. Accelerator-mode islands

The superdiffusion originates from the existence of stable accelerator modes island (AM island).[12,34–36] The AMs are generalized periodic orbits of maps having translational symmetry in phase space. The cylindrical phase space of DKR allows one to define consistently periodic orbits in a generalized version[23]

$$P_{n+x} = P_n + \pi\omega; \quad \theta_{n+x} = \theta_n, \tag{12}$$

where ω is an integer, called "jumping index".[23] For $\omega = 0$, this represents the closed periodic orbits, while for $\omega \neq 0$, the periodic orbits with x period (Eq. (12)) is an AM with acceleration $\pi\omega$. If the accelerator mode is stable, the corresponding n acceleration points are surrounded by islands. The phase point that satisfies the acceleration condition and corresponds to the island of stable acceleration is called the acceleration center. Although some islands occupy only a small fraction of the phase space, these accelerated periodic orbits dominate the diffusion of the entire phase space, such that, when there are accelerator islands in the phase space the global value of the diffusion exponent μ for the whole phase space must always converge to the value of $\langle p_t^2 \rangle \propto t^\mu$, $1 < \mu < 2$.

High-period AM islands occupy a much smaller area of phase space than period-1 and period-2 AM islands, which have less impact on global diffusion, thus only period-1 and period-2 AM islands are investigated in this paper.

First, we analytically calculate the period-1 accelerator orbits, *i.e.*, the centers of period-1 accelerator islands. Invoking map Eq. (8) we can derive

$$\begin{aligned} \Delta P_n &\equiv P_{n+1} - P_n = K\sin(\theta_n) - K\sin(\theta_n + P_n + K\sin\theta_n), \\ \Delta\theta_n &\equiv \theta_{n+1} - \theta_n = K\sin(\theta_n + P_n + K\sin\theta_n). \end{aligned} \tag{13}$$

Imposing the condition of acceleration, *i.e.*, Eqs. (12) and (13), leads to

$$\begin{aligned} &\Delta P = 2K \cdot \cos\frac{2\theta_n + P_n + K\sin\theta_n}{2} \cdot \sin\frac{P_n + K\sin\theta_n}{2} = \pi\omega, \\ &\Delta\theta = K\sin(\theta_n + P_n + K\sin\theta_n) = 0 \pmod{2\pi}. \end{aligned} \tag{14}$$

Additionally, as per Eq. (12), P_n and θ_n must be a rational multiple of π. Furthermore, when K is an integer multiple of π, the term

$$\cos\frac{2\theta_n + P_n + K\sin\theta_n}{2} \cdot \sin\frac{P_n + K\sin\theta_n}{2}$$

must also be a rational number. Thus

$$\frac{2\theta_n + P_n + K\sin\theta_n}{2} = \frac{\pi}{6}, \frac{5\pi}{6}, \frac{\pi}{2} \pmod{\pi},$$
$$\frac{P_n + K\sin\theta_n}{2} = \frac{\pi}{6}, \frac{5\pi}{6}, \frac{\pi}{2} \pmod{\pi}, \tag{15a}$$
$$\frac{2\theta_n + P_n + K\sin\theta_n}{2} = \frac{\pi}{4}, \frac{3\pi}{4} \pmod{\pi},$$
$$\frac{P_n + K\sin\theta_n}{2} = \frac{\pi}{4}, \frac{3\pi}{4} \pmod{\pi}. \tag{15b}$$

The results of the accelerator center (θ, P) for periodic-1 are as follows: For the case of K being taken an even multiple of π, we have

$$\theta = \frac{i\pi}{2}, \quad i = 0,1,2,3,$$
$$P = \frac{\pi}{2}, \frac{3\pi}{2}, \tag{16a}$$
$$\theta = \frac{\pi}{2}, \frac{3\pi}{2},$$
$$P = \pi. \tag{16b}$$

And for the case of K being taken an odd multiple of π, we have

$$\theta = \pi/2, 3\pi/2; \quad P = \pi/2, 3\pi/2. \tag{17}$$

We perform numerical simulations of accelerator centers for period-1 and period-2 when the parameter K is an even multiple of π (Fig. 2(a)) and an odd multiple of π (Fig. 2(b)). We find that period-1 accelerator orbits are in agreement with previous analytical calculations. For the case of an odd multiple of π, in addition to period-1 orbits as predicted by Eqs. (16a) and (16b), we also observed the emergence of period-2 orbits. Figure 2(a) reveals that the period-1 AM islands in DKR are not situated on the θ axis, unlike those in KR which all belong to group-II islands[23] and are located on the θ axis. The phase diagram shows that when $K = 2\pi$, DKR has 10 pairs of period-1 AM islands, which correspond to only two pairs in KR with similar parameters. The total area of the AM islands in DKR is considerably greater than that in the KR. As a result, the global diffusion coefficients D_{eff} of the DKR are between four and seven times that of KR for the same kicked intensity, particularly when K is approximately between 6.3 and 6.33.[11]

In comparison with the KR, as shown in Fig. 2(a), we can see that none of the period-1 AM islands in DKR are on the x axis (the period-1 AM islands in KR are all on the x axis and belong to group-II islands[23]). When $K = 2\pi$, The phase diagram contains 10 pairs of period-1 AM islands, corresponding to only two 2 in the KR with the same parameters, and it is clear from the phase diagram that the total area of the AM island of DKR is much larger than that of KR. This explains why the global diffusion coefficients D_{eff} of the DKR correspond to those between four and seven times of KR for the same kicked intensity when K is approximately between 6.3 and 6.33.[11]

When K is an integer multiple of π and these periodic orbits are stable, accelerator islands centered at them will form in phase space. When K is slightly larger than an integer multiple of π, these AM islands will bifurcate. In the following, we will discuss the period-1 and period-2 accelerator mode islands.

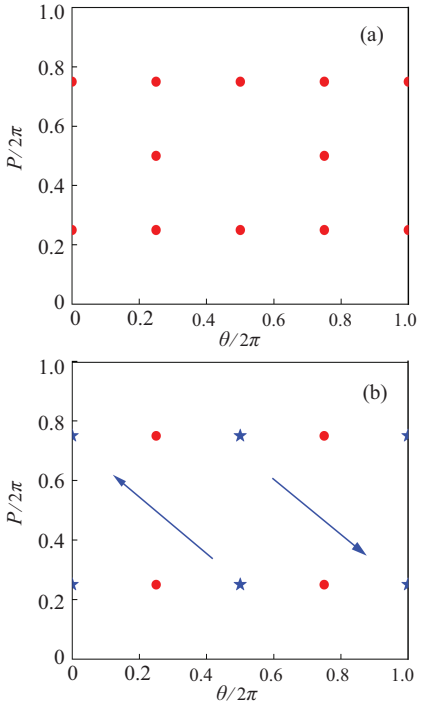


Fig. 2. (a) The position of the center of acceleration in phase space when K is taken as an even multiple of π (2π, 4π, 6π), and (b) the position of the center of acceleration in phase space when K is taken as an odd multiple of π (π, 3π, 5π). The red dots correspond to the acceleration centers of the period-1 AM islands, the blue dots correspond to the acceleration centers of the period-2 AM islands, and the blue arrows represent the direction of motion of the phase points on the period-2 islands.

3.1. Period-1 AM islands

The existence of a stable period-1 AM island is dependent on the satisfaction of the accelerator condition, as specified by Eq. (12) with $x = 1$, and the stable conditions

$$|\operatorname{tr} J_x| < 2, \quad J_x = \prod_{n=1}^{x} J_n, \tag{18}$$

where J_n denotes the n-th iterated Jacobian matrix. From these conditions, it can be deduced that the initial conditions and the parameter K must satisfy

$$K\sin(\theta_0 + P_0) = 2\pi N, \; K\sin\theta_0 = 2\pi M, \quad \omega \text{ is even},$$
$$K\sin(\theta_0 + P_0) = 2\pi N, \; K\sin\theta_0 = \pi M, \quad \omega \text{ is odd}, \tag{19}$$
$$-4 < K^2\cos(\theta_0 + P_0 + K\sin\theta_0)\cos\theta_0 < 0, \quad \omega \text{ is even},$$
$$0 < K^2\cos(\theta_0 + P_0 + K\sin\theta_0)\cos\theta_0 < 1, \quad \omega \text{ is odd}, \tag{20}$$

where M is a non-zero integer and N is any integer. The value K satisfying both Eqs. (19) and (20) can be calculated

$$0 < \left[\left(\frac{K}{2\pi}\right)^2 - M^2\right]\left[\left(\frac{K}{2\pi}\right)^2 - N^2\right] < \frac{4}{\pi^2},$$
ω is even, (21)
$$0 < \left[\left(\frac{K}{2\pi}\right)^2 - \frac{M^2}{4}\right]\left[\left(\frac{K}{2\pi}\right)^2 - N^2\right] < \frac{1}{\pi^2},$$
ω is odd. (22)

It is easy to calculate the result of the gap period of K for the emergence of the period-1 AMs when $M = N$ (for ω is even) and $M = 2N$ (for ω is odd)

$$\Delta K = \left[(2\pi M)^2 + 4\right]^{1/2} - 2\pi M \approx \left|\frac{2}{K}\right|, \tag{23}$$

for $M \neq N$ (for ω is even) and $M \neq 2N$ (for ω is odd), we can obtain

$$\Delta\frac{K}{2\pi} = \begin{cases} \left|\dfrac{M^2-N^2}{2}\right| \left(\sqrt{1+\left(\dfrac{4}{(M^2-N^2)\cdot\pi}\right)^2} - 1\right), \\ \omega \text{ is even}, \\ \left|\dfrac{M^2-N^2}{2}\right| \left(\sqrt{1+\left(\dfrac{1}{\left(\dfrac{M^2}{4}-N^2\right)\cdot\pi}\right)^2} - 1\right), \\ \omega \text{ is odd}. \end{cases} \tag{24}$$

One may approximate Eq. (24) by expansion to get

$$\Delta K \approx \begin{cases} \dfrac{8}{|M^2-N^2|\cdot\pi}, & \omega \text{ is even}, \\ \dfrac{2}{|M^2-N^2|\cdot\pi}, & \omega \text{ is odd}. \end{cases} \tag{25}$$

The theoretical results (Eq. (23)) indicate that as K gradually increases, the width of the interval ΔK decreases correspondingly. This is in agreement with the numerical results depicted in Fig. 1(b). We can see that the period-1 AM islands appears near the point where K is an integer multiple of π (Eq. (21)), when K is slightly larger than an integral multiple of π in the fetching interval, $\sin\theta_0$ will smaller than 1, stable AM islands doubly appear due to bifurcation, and the two islands are close to the accelerator center when K is the multiple of π.

Figures 3 and 4 present numerical results of the period-1 AM islands in the phase space for $K = 2\pi + 0.1$ and $K = \pi + 0.02$, respectively. Figures 3(a) and 4(b) depict the bifurcation of period-1 AM from the accelerator centers located at $(0.5\pi, \pi)$ and $(1.5\pi, 1.5\pi)$, respectively. The system's symmetry results in 4 pairs of period-1 AM islands in the phase space, bifurcating from the 4 accelerator centers (Fig. 2(b)). Similarly, there is another pair of period-1 AM islands symmetrical to Fig. 3(a) near $(1.5\pi, 0.5\pi)$. The boundaries of the period-1 AM islands exhibit complex, self-similar structures, as shown in Figs. 3(b) and 3(c), which can be explained by the Poincaré–Birkhoff theorem and reformation group theory.[15,37] These self-similar structures are characterized by nested layers of smaller islands forming chains, as exemplified in Fig. 3(b). In the range described by Eq. (21), the topology of the islands is highly influenced by variations in K.

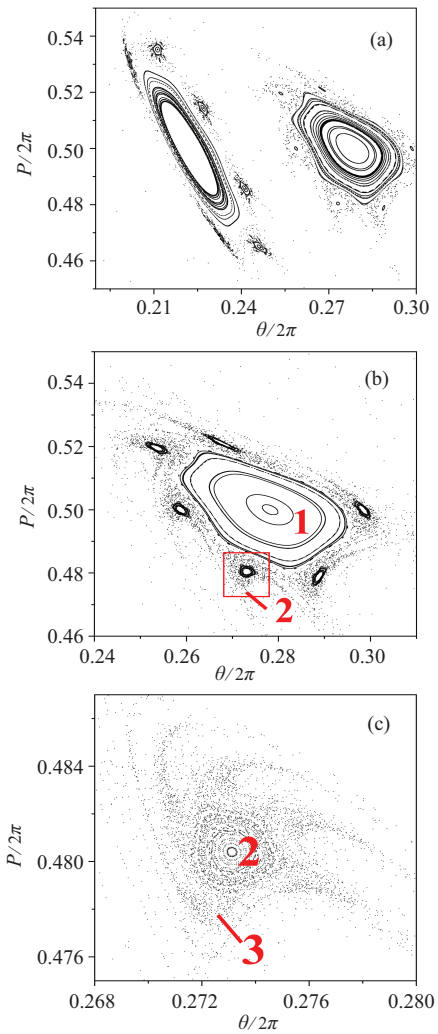


Fig. 3. At $K = 2\pi + 0.1$, (a) a pair of period-1 AM islands generated by bifurcation at $K = 2\pi$; (b)–(c) one of the AM islands in (a), the three generations of self-similar structure around the island contains a group of small islands of period-6.

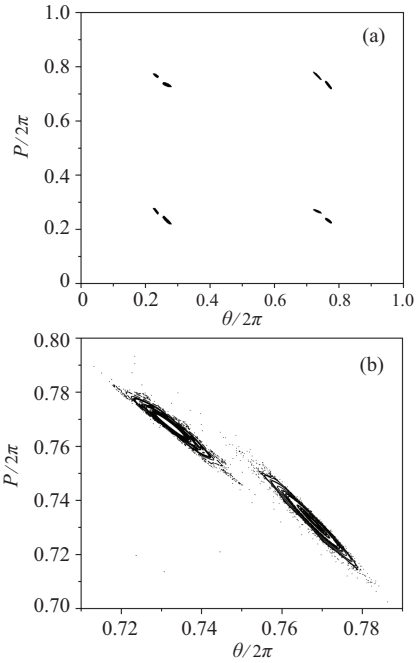


Fig. 4. At $K = \pi + 0.02$, (a) 4 pairs of period-1 AM islands generated by bifurcation at $K = \pi$ and (b) a pair of islands diverges at $(1.5\pi, 1.5\pi)$.

3.2. Period-2 AM islands

The condition of accelerator for the case of period $x = 2$ is given below:

$$\begin{cases} P_{n+2} - P_n = L_{\text{const}} = \pi A, \\ \theta_{n+2} - \theta_n = L'_{\text{const}} = 2\pi B. \end{cases} \tag{26}$$

By inserting Eq. (26) into map Eq. (8), we obtain the following expression:

$$K \sin \theta_n + K \sin \theta_{n+1} = L + L'. \tag{27}$$

Here, we only discuss the case of $L + L' = 0$, then equation (27) gives either

$$\theta_{n+1} = \pi M + \theta_n, \tag{28}$$

or

$$\theta_{n+1} = -\theta_n. \tag{29}$$

For the case $\theta_{n+1} = -\theta_n$, by substituting Eq. (29) into the map, one can obtain the relation $P_{n+2} \equiv P_n$, *i.e.*, $A = 0$, which are closed periodic orbits. For the case

$$\theta_{n+1} = \pi M + \theta_n,$$

by bringing Eq. (27) into the map, the acceleration condition can then be obtained as follows:

$$\begin{aligned} &K \sin(\theta_0 + P_0 + K \sin \theta_0) = \pi N, \\ &K \sin \theta_0 = \pi M. \end{aligned} \tag{30}$$

The stability condition (*e.g.* Eq. (18)) for the period-2 orbits can be rewritten as

$$|1 - T_1 - T_2 + T_2 C_1 - T_1 C_2 + T_1 T_2 C_1 C_2| < 2, \tag{31}$$

where

$$\begin{cases} C_i = K \cos \theta_i, \\ T_i = K \cos(\theta_i + \mathrm{P}_i + K \sin \theta_i). \end{cases} \tag{32}$$

The value K satisfying both Eqs. (30) and (31) demands

$$\left|1 - 2T_3 + 2T_3 T_4 - T_3^2 T_4^2\right| < 2, \tag{33}$$

in which

$$\begin{cases} T_3 = \sqrt{K^2 - (\pi M)^2}\sqrt{K^2 - (\pi N)^2}, \\ T_4 = \sqrt{K^2 - (\pi N)^2}. \end{cases} \tag{34}$$

It is followed from Eq. (33) that the period-2 AM islands appear near the point where K is an integer multiple of π. As shown in Fig. 5, similar to Fig. 4, the period-2 AM island also surrounded by the self-similar structure, the chain structure consists of six small islands.

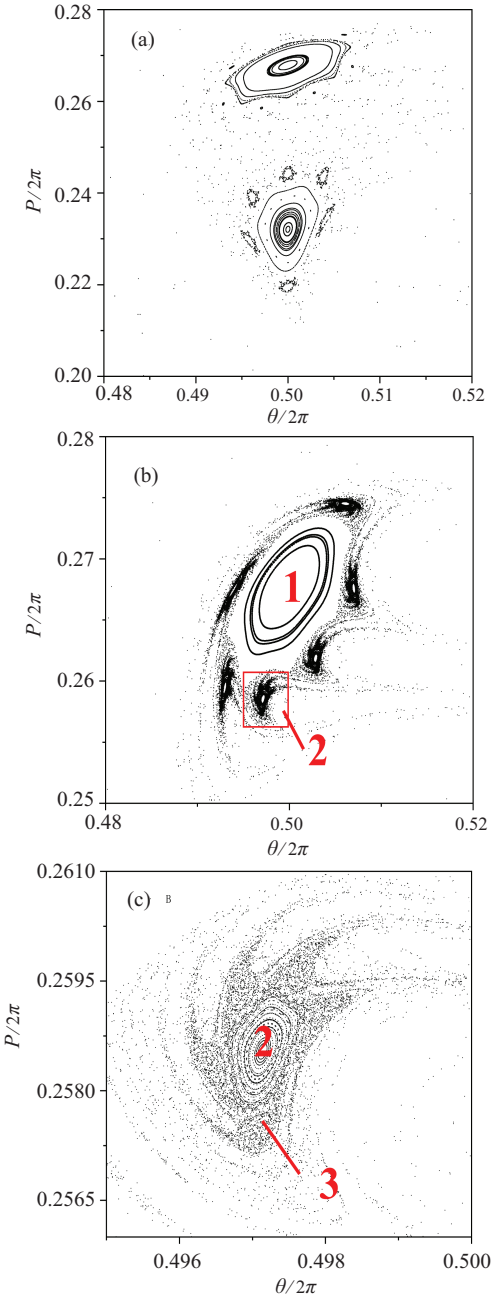


Fig. 5. A pair of period-2 AM island in phase space at $K \approx 3.16$. (a) The distribution of this trajectory in phase space. (b)–(c) One of the AM islands in panel (a), three generations of the self-similar structure around the island contains a group of small islands of period-6.

4. Dynamics in the stickiness region and stickiness time

The "stickiness time", also referred to as the "escape time", is a measure of the amount of time required for an orbit to move away from its initial conditions into the larger chaotic region. When the initial conditions of an orbit are outside and close to the outermost KAM curve of a stable island, the orbit can become trapped around the island for a prolonged period of time due to the presence of cantori, or cantori sets of points surrounding the islands of stability. Chaotic orbits are forced to move close to and along the unstable manifolds of the unstable periodic orbits in this region. Given that these manifolds

undergo multiple foldings before exiting the holes in the cantori, chaotic orbits spend a significant amount of time around these islands before finally escaping into the larger chaotic region, far from the islands of stability.[7,8]

Figure 6 illustrates how the average energy of the phase points in the stickiness region varies with the number of iterations n. The phase point energy undergoes a transition from: superdiffusion, to localization and finally to normal diffusion (provided that no other island effects are received). This means that the phase point escapes the stagnant region and enters the sea of chaos.

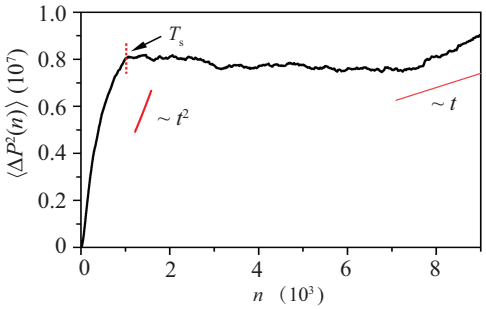


Fig. 6. The evolution of $\langle \Delta P^2(n) \rangle$ as a function of the number of iterations n, in a double logarithmic scale. The slope of this curve corresponds to the diffusion exponent μ. The initial condition is to uniformly select 10^4 points in a square located in the stickiness region.

An orbit located outside the outermost KAM curve of a stable island may experience a prolonged stay in the vicinity of the island due to the presence of cantori. This behavior, characterized by the time it takes for the orbit to escape, known as the stickiness time, which is indicated by the arrow in Fig. 6, can be used to quantify the ballistic diffusion and provide insight into the system's complexity. Stickiness time has been related to measures such as the fractal dimension and diffusion exponent in previous studies.[18] In this work, we explore the stickiness time in the context of the double-kicked rotor.

We classify phase points in the phase space of the double-kicked rotor into three categories: those in the chaotic sea, with short stickiness times (T_s), those on the KAM islands, with infinite stickiness times, and those in the stickiness region, with intermediate T_s. As an example, We find that the scaling law of $T_s(R)$ changes as R varies. As shown in Fig. 7(a), red regions and white regions represent T_s of infinity and T_s smaller than 20, respectively. The comparison between Fig. 7(a) and Fig. 3 reveals that the red regions correspond to the KAM islands and the white regions correspond to the chaotic sea, while the remaining regions correspond to the stickiness region. Thus, we categorize the initial conditions according to the magnitude of T_s, which serves as an effective descriptor of the dynamics of phase points.

We calculated the radius R of the phase points corresponding to the different average stickiness times, where the radius R defined as the distance from the acceleration center $(\pi - \arcsin 2\pi/6.3832, \pi)$ to the phase point. A curve between the average stickiness time and the corresponding radius can be obtained as in Fig 7(b). Clearly, we can see, as R increases, same as the regular islands,[38] $\bar{T}_s$ will first undergo an exponentialy decay in the red regions (Fig. 7), but after that it will undergo a power-law decay in the stickiness regions.

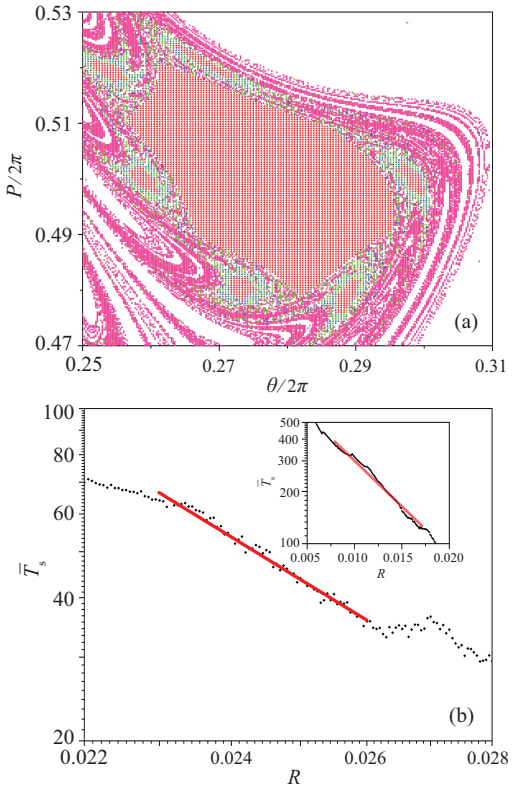


Fig. 7. At $K = 6.3832$, (a) the phase diagram is divided into different regions according to the stickiness time, where the red region corresponds to the initial conditions for the region of infinite stickiness time, and the blue, green, and yellow regions correspond to the initial conditions for stickiness times between [800–1000], [300–800], and [100–300], respectively. The pink region with a very distinct boundary corresponds to an initial condition with a stickiness time between [20–100]. (b) The stickiness time T_s for each initial condition in the pink region corresponds to the average of distance from the acceleration center R for different initial conditions at the same stickiness time in double logarithmic coordinates. The range for selecting the initial conditions lies in the pink area, *i.e.*, 10^4 initial conditions with stickiness times between 20 and 100 are selected uniformly, plotted in the logarithmic coordinate system. The phase points in the upper right-hand vignette correspond to those located in the red area, in semi-logarithmic coordinates.

That the stickiness time decreases significantly as R increases. We obtain the fitting relationship

$$T_s \sim R^{-5}. \tag{35}$$

The R range of 0.046π to 0.052π approximately corresponds to the pink area, with numerical results presented in Fig. 7(b).

5. Discussion and summary

This paper investigates the mechanism underlying superdiffusive behavior in DKR systems, which is the presence of AM islands in the phase space. We first established the conditions for the existence of period-1 acceleration centers

through theoretical calculations. These acceleration centers occur near integer multiples of the system parameter $K = \pi$, and have different distributions corresponding to odd or even multiples of K equal to π. Both distributions alternate with a period of $\Delta K = 2\pi$. The locations of these acceleration centers generate islands of stability in the vicinity, and the phase points inside the islands as well as the stickiness regions in the vicinity of the islands affect the global diffusion across the phase space. Comparing the DKR system to the KR system reveals that the DKR system has five times more period-1 AM islands when the same system parameters are present and superdiffusion occurs. This is due to the fact that the global diffusion coefficient is proportional to the area of the AM islands.[11]

In addition, we calculated the conditions for the stable existence of the two types of AM islands in the phase space that have the greatest influence on diffusion: the period-1 AM islands and the period-2 AM islands. We offer a thorough analysis of local diffusion within the islands and at their boundaries, as well as the global diffusion influenced by their presence. In this case, the period-1 AM island will be in the vicinity of an integer multiple of K equal to π, while the period-2 AM island exists only in the vicinity of an odd multiple of K equal to π. Structures with self-similar island chains exist in the vicinity of the islands, and the number of islands in the chain is strongly influenced by changes in the value of K.[37]

We also noted that an orbit with initial conditions outside and close to the last KAM curve of an island of stability can be trapped for a long time around this island due to the appearance of cantori. The stickiness region near the island is the second most influential region for global diffusion, apart from the phase point inside the island. Therefore, we further develop the discussion of the dynamics of the stickiness region in a DKR system and the stickiness time in the last section. Phase points located in the stickiness regions undergo a transition from superdiffusion to localization and finally to normal diffusion (provided that no other island effects are received). This implies that the phase point escapes the stagnant region and enters the sea of chaos. Taking $K = 6.3832$ as an example, we calculated the radius R of the phase points corresponding to different average stickiness times. The mean stickiness time decays exponentially when the phase point is located within the island, and once the phase point enters the stickiness region, it undergoes a power-law decay with a power of approximately 5.

In summary, global superdiffusion occurs in the pseudo-classical double rotor system near rational values of K equal to π, which is attributed to the presence of stable AM islands in phase space. We also demonstrated the structural characteristics of these acceleration islands and the dynamic properties of the sticky regions surrounding them.

Further investigation is needed to determine if the AM islands exist in DKR for all values of η/τ. For instance, when $\eta/\tau \ll 1$, chaotic waves can emerge in phase space, and a region where the KAM tori are reconstructed can be found irrespective of the strength's magnitude. The influence of KAM tori on superdiffusion should be elucidated in the following research.

Acknowledgements

Project supported by the National Natural Science Foundation of China (Grant No. 12005024), the Fundamental Research Funds for the Central Universities (Grant No. 2019XD-A10), and the High-performance Computing Platform of Beijing University of Posts and Telecommunications.

References

[1] Dana I and Fishman S 1985 *Physica D* **17** 63
[2] Chirikov B V 1979 *Phys. Rep.* **52** 263
[3] Izrailev F M 1990 *Phys. Rep.* **196** 299
[4] Haake F 2001 *Quantum Signatures of Chaos* (Berlin: Springer)
[5] Karabanov A and Morozov A 2014 *Chaos, Solitons and Fractals* **69** 201
[6] Rechester A B and White R B 1981 *Phys. Rev. Lett.* **81** 4044
[7] Cary J R, Meiss J D and Bhattacharjee A 1981 *Phys. Rev. A* **23** 2744
[8] Karney C 2005 *Physica D* **8** 360
[9] Ishizaki R, Horita T, Kobayashi T and Mori H 1991 *Prog. Theor. Phys.* **85** 1013
[10] Ouchi K, Mori N, Horita T and Mori H 1991 *Prog. Theor. Phys.* **85** 687
[11] Harsoula M and Contopoulos G 2018 *Phys. Rev. E* **97** 022215
[12] Manos T and Robnik M 2014 *Phys. Rev. E* **89** 022905
[13] Wallis G 2010 *Springer* **60** 547
[14] Benkadda S, Kassibrakis S, White R B and Zaslavsky G M 1997 *Phys. Rev. E* **55** 4909
[15] Meiss J D 1980 *Phys. Rev. A* **34** 2375
[16] Birkhoff and D G 1913 *T. Am. Math. Soc.* **14** 14
[17] Birkhoff G D 1926 *Acta Mathematica* **47** 297
[18] Harsoula M, Karamanos K and Contopoulos G 2019 *Phys. Rev. E* **99** 032203
[19] Zaslavsky G M and Meiss J 1999 *Physics of Chaos in Hamiltonian systems* (London: Imperial College Press)
[20] Contopoulos G 1971 *Astron. J.* **76** 147
[21] Efthymiopoulos C, Contopoulos G and Voglis N 1999 *Int. Astron. Union Colloq.* **73** 221
[22] Lozej R, Lukman D and Robnik M 2021 *Phys. Rev. E* **103** 012204
[23] Barash O and Dana I 2007 *Phys. Rev. E* **75** 056209
[24] Li W, Chen S G and Wang G R 2001 *Phys. Lett. A* **281** 334
[25] Wang J and Gong J 2008 *Phys. Rev. A* **77** 031405
[26] Zhou L and Gong J 2018 *Phys. Rev. A* **97** 063603
[27] Tao M A and Shu-Min L I 2008 *Chin. Phys. Lett.* **25** 1968
[28] Fishman S, Guarneri I and Rebuzzini L 2002 *Phys. Rev. Lett.* **89** 084101
[29] Fang P and Wang J 2016 *Sci. China: Phys., Mech. Astron.* **59** 7
[30] Wang J, Guarneri I, Casati G and Gong J 2011 *Phys. Rev. Lett.* **107** 234104
[31] Bi H, Qi G, Hu J and Wu Q 2020 *Chin. Phys. B* **29** 020502
[32] Zhao W L and Jie Q 2020 *Chin. Phys. B* **29** 080302
[33] Stocklin M M A and Monteiro T S 2005 *Phys. Rev. E* **74** 026210
[34] Godun R M, D'Arcy M, Oberthaler M K, Summy G S and Burnett K 2000 *Phys. Rev. A* **62** 013411
[35] Rom-Kedar V and Zaslavsky G 1999 *Chaos* **9** 697
[36] Meiss J D, Miguel N, Simó C and Vieiro A 2018 *Nonlinearity* **31** 5615
[37] Iomin A, Fishman S and Zaslavsky G 2002 *Phys. Rev. E* **65** 036215
[38] Contopoulos G and Harsoula M 2010 *Int. J. Bifurcation Chaos* **20** 2005